物 理 化 学 学 报

Acta Phys. -Chim. Sin. **2023,** *39* (10), 2307046 (1 of 10)

[Article] doi: 10.3866/PKU.WHXB202307046 www.whxb.pku.edu.cn

Submicron-Sized, High Crystalline Graphene-Reinforced Meta-Aramid Fibers with Enhanced Tensile Strength

Zhenfei Gao [1,3,†], Qingquan Song [2,†], Zhihua Xiao [1,3,4,†], Zhaolong Li [1,3,5], Tao Li [3], Jiajun Luo [1,3], Shanshan Wang [1], Wanli Zhou [6], Lanying Li [1,6], Junrong Yu [2,*], Jin Zhang [1,3,*]

[1] School of Materials Science and Engineering, College of Chemistry and Molecular Engineering, Academy for Advanced Interdisciplinary Studies, Beijing Science and Engineering Center for Nanocarbons, Peking University, Beijing 100871, China.

[2] State Key Laboratory for Modification of Chemical Fibers and Polymer Materials, College of Materials Science and Engineering, Donghua University, Shanghai 201620, China.

[3] Division of Graphene Fiber Technology, Beijing Graphene Institute, Beijing 100095, China.

[4] State Key Laboratory of Heavy Oil, China University of Petroleum, Beijing 102249, China.

[5] State Key Laboratory of High-efficiency Coal Utilization and Green Chemical Engineering, College of Chemistry and Chemical Engineering, Ningxia University, Yinchuan 750021, China.

[6] China Bluestar Chengrand Co., Ltd., Chengdu 610000, China.

Abstract: Aramid fiber is highly regarded for its outstanding properties and is widely used in various industrial applications. Among the different types of aramid fibers, meta-aramids, particularly poly(m-phenylene isophthalamide) (PMIA), are known for their exceptional flame retardance, high-temperature resistance, excellent electrical insulation, and remarkable chemical stability. As a result, PMIA-based materials find extensive use in industries focused on fire prevention, heat protection, and related applications. However, PMIA fibers have limitations due to the lack of conjugation between amide and benzene ring bonds in their molecular structure, resulting in flexible segments with low crystallinity, which in turn leads to inferior mechanical strength. Researchers have shown great interest in nanocomposites as a means to overcome these limitations. In this context, graphene nanocomposites have gained significant attention. Graphene, with its benzene ring arrangement within its layers, easily bonds with polymers possessing a similar structure. This property makes graphene a promising candidate for enhancing the mechanical strength of aromatic polymers like PMIA. Moreover, small-sized graphene particles exhibit superior dispersibility within fibrous polymer matrices, leading to more effective reinforcement compared to larger graphene sheets. Consequently, incorporating high-quality, small-sized graphene into polymer matrices can substantially improve the properties of these polymers. There is a growing demand for enhancing the mechanical characteristics of aramid fibers to expand their applications beyond traditional uses. This research demonstrates how sub-micron-sized graphene improves the structural integrity and mechanical strength of PMIA fibers. The results show a remarkable 46% enhancement in tensile strength compared to unmodified PMIA fibers. While the graphene/PMIA fiber exhibits exceptional mechanical properties, it also holds great potential for applications in wearables, flexible sensors, and various other domains, thanks to graphene's versatile characteristics. This research underscores the importance of utilizing small-sized, high-quality graphene to develop more robust carbonaceous nanocomposite fibers suitable for a wide range of commercial purposes. Beyond its immediate impact on PMIA fibers, this

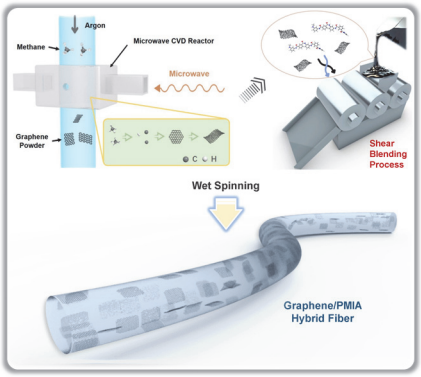

Received: July 24, 2023; Revised: September 7, 2023; Accepted: September 8, 2023; Published online: September 12, 2023.

†These authors contributed equally to this work.

*Corresponding authors. Emails: yjr@dhu.edu.cn (J.Y.); jinzhang@pku.edu.cn (J.Z.); Tel.: +86-10-62752555 (J.Z.).

The project was supported by the Ministry of Science and Technology of China (2022YFA1203302, 2022YFA1203304, 2016YFA0200100), National Natural Science Foundation of China (52021006, 51720105003, 21790052, 52102035), Strategic Priority Research Program of CAS (XDB36030100), Beijing National Laboratory for Molecular Sciences (BNLMS-CXTD-202001), and Science Foundation of China University of Petroleum (Beijing) (ZX20230047).

国家科技部(2022YFA1203302, 2022YFA1203304, 2016YFA0200100), 国家自然科学基金(52021006, 51720105003, 21790052, 52102035), 中国科学院战略性先导科技专项(XDB36030100), 北京分子科学国家研究中心(BNLMS-CXTD-202001)及中国石油大学(北京)科学基金(ZX20230047)资助项目

research represents a significant step forward in advancing the utilization and growth of graphene materials in various applications.

Key Words: Sub-micron-sized graphene; Meta-aramid fiber; Shear dispersion; Tensile strength; Internal structure optimization

亚微米尺寸、高结晶度石墨烯增强间位芳纶纤维力学性能

高振飞[1,3,†]，宋清泉[2,†]，肖志华[1,3,4,†]，李兆龙[1,3,5]，李涛[3]，罗家俊[1,3]，王珊珊[1]，周万立[6]，李兰英[1,6]，于俊荣[2,*]，张锦[1,3,*]

[1]北京大学材料科学与工程学院，化学与分子工程学院，前沿交叉学科研究院，北京市低维碳材料科学与工程技术研究中心，北京 100871

[2]东华大学材料科学与工程学院，纤维材料改性国家重点实验室，上海 201620

[3]北京石墨烯研究院，石墨烯纤维技术研究部，北京 100095

[4]中国石油大学(北京)，重质油国家重点实验室，北京 102249

[5]宁夏大学化学化工学院，省部共建煤炭高效利用与绿色化工国家重点实验室，银川 750021

[6]中蓝晨光化工研究设计院有限公司，成都 610000

摘要：芳纶纤维具有优异的综合性能，在各种工业应用中备受青睐。其中，间位芳纶纤维，也称聚间苯二甲酰间苯二胺(PMIA)纤维，兼具阻燃、耐高温、电隔离和高化学稳定性。其织物材料广泛应用于防火、防热等行业。然而，由于分子链中酰胺和苯环键之间缺乏偶联，内旋能低，导致PMIA纤维链段柔软、结晶度低，展现出较低的机械强度。因此，迫切需要改善这些纤维的机械特性，以扩大其应用范围。纳米复合材料的可以赋予基体材料许多独特特性。其中，石墨烯纳米复合材料占据突出地位。石墨烯面内的苯环结构使其可以有效增强芳香族和脂肪族类聚合物材料。此外，与大尺寸的石墨烯相比，小尺寸的石墨烯在聚合物基体中表现出更好的分散性，可在纤维类聚合物材料中展现出更明显的增强效应。因此，使用高品质、小尺寸的石墨烯是增强聚合物基体的有效手段。我们的研究展示了亚微米尺寸的石墨烯如何改善PMIA纤维的结构完整性和增加机械强度。结果显示，与未改性的PMIA纤维相比，拉伸强度显著提高46%。鉴于该方法的有效性，可以采用此种“小尺寸、高品质”的石墨烯来开发更强韧且更具商用价值的碳基纳米复合纤维。

关键词：亚微米级石墨烯；间位芳纶纤维；剪切分散；拉伸强度；内部结构优化
中图分类号：O649

1 Introduction

Meta-aramid fibers are organic fibers with excellent comprehensive properties [1], such as high-temperature resistance, electrical isolation, *etc*. Since DuPont realized the industrial production of Nomex in the 1960s, the global market scale of meta-aramid has exceeded 40000 tons per year [2]. Meta-aramid fibers have become indispensable basic materials in high-tech industries such as aerospace, military fire protection, energy conservation, environmental protection, and petrochemical industries [3–7]. The meta-aramid polymer solution is prepared by low-temperature polycondensation of meta-phenylenediamine and isophthaloyl chloride, and its molecular chain is a linear macromolecule composed of amide groups connected to meta-phenyl groups [8]. Due to the lack of conjugation between the amide and benzene ring bonds in the molecular chain, and the low internal rotation energy, the poly(m-phenylene isophthalamide) (PMIA) fiber segment has good flexibility and low crystallinity [9,10]. Meanwhile, plenty of hydrogen bonds between the meta-aramid molecular chains [11], improve the stability of meta-aramid fibers to a certain extent but also lead to weaker lateral interactions between polymer chains [8]. With the increasingly demanding application scenarios, more stringent requirements have been put forward on the mechanical properties of meta-aramid fibers [12]. The meta-aramid fiber prepared by wet spinning has inherent internal defects, such as the core-sheath structure during the solidification process, internal pores, and low crystallinity and orientation caused by the stretching orientation process [13]. It is relatively limited to improve the mechanical properties of meta-aramid fibers through process optimization which is mainly contributed from the regularization of fiber crystallinity and orientation. However, the way of monomer modification is prone to mismatch with the current polymerization and spinning process and causes the deterioration of the PMIA fibers' intrinsic properties. Therefore,

it is important to improve the mechanical properties of meta-aramid fiber, but it must be based on matching mature preparation process conditions and ensuring the inherent excellent properties of the meta-aramid fiber.

Graphene has excellent intrinsic mechanical properties (tensile strength of 130 GPa, Young's modulus of 1.0 TPa, and huge specific surface area), and has long been regarded as an ideal nano-reinforced material for high-performance and advanced functional polymer materials [14–16]. Firstly, the addition of graphene can enhance the lateral interaction of polymer chains in aramid fiber through π–π interaction [17]. Secondly, the large specific surface area of graphene gives it more contact interfaces with polymer molecules, which is conducive to serving as a load-bearing unit during the fracture process and thus improving the mechanical properties of the composite fiber [18]. In addition, based on graphene's excellent flexibility and thermal properties, it can perfectly meet the high thermal protection and wear requirements of meta-aramid [19–21]. However, graphene's excellent dispersibility and reasonable size matching are the basis for ensuring the above enhancement effect. Graphene oxide with rich surface functional groups has better dispersibility than graphene in the polymer matrix, but its crystal structure was severely damaged in the functionalization process, which resulted in a serious decline in mechanical properties [22]. Moreover, the size of the more commonly used graphene materials is usually above 1 μm, and it is easier to form defects than to strengthen in the smaller diameter aramid fiber monofilament (10–15 microns). Therefore, the preparation of graphene with a small size, suitable dispersibility, and excellent intrinsic properties is the key to strengthening aramid fiber.

Here, our experiment demonstrates that using graphene produced *via* microwave plasma chemical vapor deposition (MPCVD) to modify PMIA fibers can yield impressive improvements in their mechanical properties [23]. By combining solution blending and shear dispersion techniques, we achieved exceptionally homogeneous dispersions of graphene within the PMIA fiber matrix. This approach allows for strong intermolecular bond formation between PMIA molecules and reduces internal porosity, resulting in greater crystallinity and enhanced fiber orientation [24]. Under tensile loading, the graphene-PMIA interface facilitates efficient stress transfer, leading to a notable 46% increase in radial tensile strength compared to non-graphene-modified PMIA fibers [25]. Our findings offer valuable insights into the development of advanced aramid composite materials through the judicious inclusion of graphene reinforcements.

2 Experimental section

2.1 Materials

PMIA solution with a solid content of 18.5% was supported by X-Fiper New Material Co., Ltd. DMAc (Analytical Reagent, AR) and PVP (polyethylene pyrrolidone) (AR) were purchased from Sinopharm Group Chemical Reagent Co., Ltd.

2.2 Preparation of graphene and graphene dispersions

Continuous "snowing" graphene *via* pulse-etched process: a surface wave type of plasma was created in the center of a quartz tube with an internal diameter of 22 mm. The maximum power of the microwave (2.45 GHz) provided by a generator (Sairem, France) was 2 kW. Argon (800–5000 $cm^3 \cdot min^{-1}$ (at standard temperature and pressure, STP)) was introduced into the tube to expel the residual air and then initiate the plasma at ambient pressure. A nominal amount of methane (2–20 $cm^3 \cdot min^{-1}$ (at STP)) was brought into the system for graphene preparation in the gas phase. After a 20–30 min reaction, the inner wall of the tube was partially covered with black graphene. Then, replaced methane with oxygen (5–10 $cm^3 \cdot min^{-1}$ (at STP)) to etch the wrapped graphene for 1–5 min, alternating methane, and oxygen for continuous "snowing" graphene. Graphene powder could be obtained downstream or on the tube wall.

We opted for using anhydrous DMAc as our solvent to produce the graphene dispersion. To do so, we first subjected the graphene powder to mechanical mixing with the DMAc while being shielded from the environment by nitrogen. Next, we pre-dissolved PVP in the DMAc before combining them under vigorous shearing forces generated by an Ultrasonic Cell Crusher (kHz) with 800 W power. After thorough mixing, we acquired a homogeneous dispersion having a final graphene concentration of 3%.

2.3 Preparation of graphene/PMIA blend solutions

Using a three-neck flask, we introduced PMIA solution (solids content: 18.5%) along with graphene dispersions featuring 3% mass fractions. While maintaining a steady flow of dry nitrogen throughout the process, a Teflon stirring paddle was used to mix everything thoroughly over a period of 3 h until a consistent color had been achieved. Subsequently, this mixture was processed through a triple roll mill (TR80A TRILOS model, United States) equipped with a 3 μm slit gap. Three passes were performed in total to achieve optimal consistency. In spite of the elevated dynamic viscosity caused by the high surface area of graphene, restricting the graphene/PMIA polymer mass ratio to approximately 18% helps uphold adequate liquidity during the spinning procedure. Our investigation focused on assessing the impacts of diverse graphene concentrations, which involved testing four categories with respective graphene proportions of 0, 0.5, 1.0, and 1.5 wt%.

2.4 The wet spinning of graphene/PMIA fibers

A lab-scale wet spinning line was assembled to produce the graphene/PMIA fibers. At 40 °C, the graphene/PMIA blend solutions were degassed and extruded through the spinneret containing 50 holes with a diameter of 0.08 mm and entered into a coagulation bath containing 50% DMAc and solidified into fibers under the draw ratio of 0.5. Then the fibers entered into a water bath and stretched with a ratio of 2 under 80 °C, finally washed in a water bath at 60 °C and collected. The collected fibers were soaked in water at 60 °C to remove residual solvent

and subsequently, the fibers were dried at 60 °C to remove residual moisture. The dried fibers were stretched a certain number of times in the heat pipe at 300 °C [26,27].

2.5 Characterizations

The rheology of all solutions was measured on a rotational rheometer (Physica MCR 302, Anton Paar, Austria). The 50 mm diameter concentric parallel plate geometry was used and the gap was 1 mm. Steady shear measurements were tested at a shear-rate range from 0.1 to 100 s^{-1}, and the chosen temperature was 40 °C. Frequency sweep measurements were tested at a range from 100 to 0.1 rad·s^{-1}. Before this test, a dynamic strain sweep was performed at the frequency of 6.3 rad·s^{-1}, and the linear viscoelastic regime was obtained. And the strain of 5% was within a linear viscoelastic regime, which was a set-strain amplitude for the frequency sweep measurement.

The mechanical properties of the fibers were tested by a fiber mechanical strength tester (XQ-1, China). The stretching rate was 30 mm·min^{-1} with a 20 mm gauge length. The tensile strength and elongation at break were calculated as the average of at least 30 measurements from stress–strain curves.

The crystalline structure of all graphene/PMIA fibers was evaluated by powder X-ray diffraction (XRD) tests (Bruker D8 ADVANCE, Bruker D8, Germany), and XRD patterns were obtained over the 2θ range of 5°−60°. The 2D-WAXD measurements were tested on the Bruker D8 Discover Bruker system using an incident Cu-K_α X-ray beam perpendicular to the fiber axis for evaluating the orientation degree of fibers. The radially averaged and azimuthal intensity profiles of the principle diffraction peaks were extracted from every 2D-WAXD image. The PMIA and graphene/PMIA fibers were organized into a neat bundle of filaments with a length of 30 mm and diameter of 3 mm to conduct the orientation test and Herman orientation factor (f_c). The X-ray wavelength is 0.154 nm, and the distance between the detector and fibers is 10 mm.

The SCY-3 type sound velocity orientation meter was used to measure the sonic orientation of fiber (f_s). The experiment was repeated 5 times to get the average value fiber orientation factor calculated according to Eq. (1). Where C and C_u are the sound velocities of fiber samples and polypropylene amorphous fibers, respectively.

$$f_s = 1 - C_u^2/C^2 \quad (1)$$

Scanning electron microscope (SEM) of the PMIA fiber and graphene/PMIA blend fibers was taken on a scanning electron microscope (Hitachi SU8010, Japan). Limiting oxygen index (LOI) measurement was undertaken by an oxygen index apparatus (JF-3, China) according to GB/T 5454.

Thermal stabilities of the graphene/PMIA fibers were analyzed using TA Instruments. The graphene/PMIA fibers were heated at 20 °C·min^{-1} within a range of 50–800 °C under the nitrogen atmosphere (TG 209 F1 Iris, Germany). Thermal dynamic mechanical behaviors of composite fibers were recorded on a dynamic mechanical analysis (DMA) system of Q800 with the temperature from 50 to 360 °C. The frequency used was 1.0 Hz and the heating rate was 5 °C·min^{-1}.

A Leica EM UC6 Ultramicrotome (United States) was employed to cut a single 1.0 wt% graphene/PMIA fiber into sections with a thickness of 50 nm. Aiming for improved flatness in the sample, the ultramicrotome's cutting rate was set at 0.1 mm·s^{-1}. Afterward, these thin sections underwent examination *via* transmission electron microscopy (TEM) utilizing an FEI Tecnai F30 (United States) microscope operating at an accelerating voltage of 300 kV. The Raman spectroscopy of graphene/PMIA fibers was investigated by Horiba LabRAM HR Evolution (Japan) with a laser wavelength of 633 nm.

To measure the surface hydrophobicity of graphene/PMIA fibers, we utilized a video-optical contact angle measuring instrument (Dataphysics OCA200, Germany). We employed the sessile drop method with an injection volume of 30 pL to determine the contact angle.

Fiber resistance to UV radiation testing was performed by exposing the fibers to a UV light source (365 nm, 24 W, Shanghai Jihui Test Equipment Co., Ltd., Shanghai, China). The fibers were exposed to the light source at a height of 100 mm for 216 h at 50% relative humidity. The tensile strength and elongation at break of the original fibers and the fibers after 9 days of exposure to UV light were measured separately under the same conditions, and the tensile strength retention rate (F_r) and elongation at break retention rate (E_r) were calculated according to the equation (2) and equation (3), respectively. F_0 and E_0 represent the tensile strength and elongation at the break of the original fiber, and F_9 and E_9 represent the tensile strength and elongation at the break of the fiber after 9 days of exposure to UV light, respectively.

$$F_r = F_9/F_0 \times 100\% \quad (2)$$

$$E_r = E_9/E_0 \times 100\% \quad (3)$$

3 Results and discussion

The graphene preparation experiment was performed in an atmospheric pressure microwave (2.45 GHz) reaction chamber. Similar to our previous work, graphene was grown directly in the gas phase, that is, "snowing," without any catalyst or substrate when introducing carbon sources such as methane in the Ar (Argon) plasma [23,28]. By using the "pulse-etching" technology to achieve continuous "snowing" graphene (Fig. 1a). The introduction of the carbon sources and the etchant is performed alternately in a pulsed manner. After growing graphene for a while, the reaction gas is switched to the etchant. Therefore, continuous "snowing" graphene in a "growth-etch-growth-etch" manner can be achieved by the simplest replacement of the reaction gas atmosphere, which is conducive to large-scale production of graphene at a low cost. Based on the 10.46% graphene yield of this technology, we can harvest submicron-sized (50–300 nm, Fig. 1b) graphene powders (Fig. S1a, Supporting Information) with excellent quality (Fig. 1c), exhibiting high C/O ratio around 85.9 (Fig. S2), and a thickness around 5 layers (Figs. S3, S4). The fiber mechanism diagram

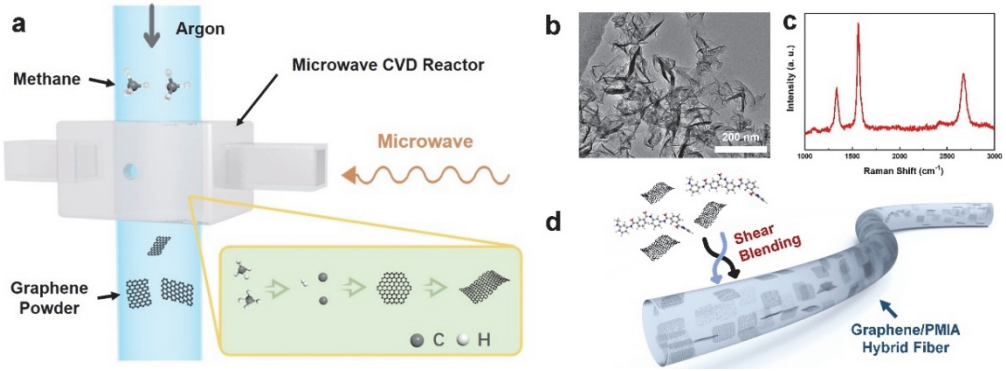

Fig. 1 (a) Scheme of the microwave-induced graphene fabrication process; (b, c) Low-magnification TEM image and the corresponding Raman spectrum of the as-prepared graphene powder; (d) Schematic diagram of the graphene/PMIA fiber. Graphene displays monodispersity in the aramid fiber matrix.

shown in Fig. 1d demonstrates the blending of graphene nanosheets in the PMIA fiber in an excellent monodisperse form.

The obtained graphene powder was dispersed in DMAc (*N*,*N*-dimethylacetamide) solution to obtain a graphene/DMAc dispersion with a concentration of 3% (Fig. S1b). Upon combining graphene dispersion and PMIA polymeric solution, they are vigorously agitated under protective inert gas. This leads to the creation of a uniform composite polymeric solution that is then subjected to three-roll processing for optimal dispersion of the graphene/PMIA polymer solutions (Figs. S5, S6). Following these steps, the blend polymer solution is deaired and spun into graphene/PMIA fibers with different graphene contents (Figs. S7, S8). To evaluate the distribution characteristics of graphene in the aramid matrix, the graphene /PMIA fibers were sliced and characterized by the TEM (transmission electron microscopy). Meanwhile, it can be seen from the cross-sectional TEM images of graphene/PMIA fibers (Fig. 2a,b) that the graphene nanosheets are uniformly distributed in the PMIA matrix in the form of scattered points. The size distribution of graphene in the PMIA matrix was consistent with that in the dispersion solution, confirming that no agglomeration occurred during the blending process of graphene and PMIA. Graphene in PMIA fibers can increase intermolecular chain lateral forces through π–π interactions. From the cross-section and surface SEM (scanning electron microscopy) images of graphene/PMIA fibers shown in Fig. 2c,d,e, we can realize that the presence of graphene leads to an effective reduction of defects in PMIA fibers, especially after heat drawing, The density of the graphene/PMIA fiber is significantly improved, which is also reflected in the reduction of the fiber diameter to a certain extent.

Rheological properties play a crucial role in determining the processability and final fiber characteristics of polymers.

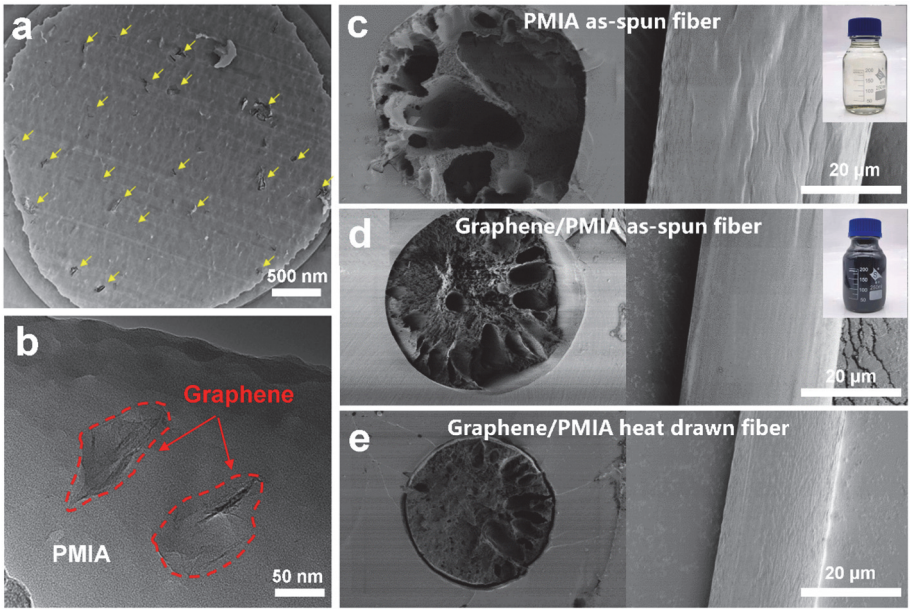

Fig. 2 (a) TEM images of the cross-section panel of graphene/PMIA fiber. The yellow arrows highlight the presence of graphene with uniform dispersion; (b) HRTEM image showing detaile morphology of graphene dispersed in PMIA matrix; (c–e) SEM images of the cross-section and surface of the PMIA as-spun fiber, 1% graphene/PMIA as-spun fiber, and 1% graphene/PMIA fiber after heat drawing. Insets: optical photographs of PMIA polymerization solution (c) and graphene/PMIA blend polymerization solution (d).

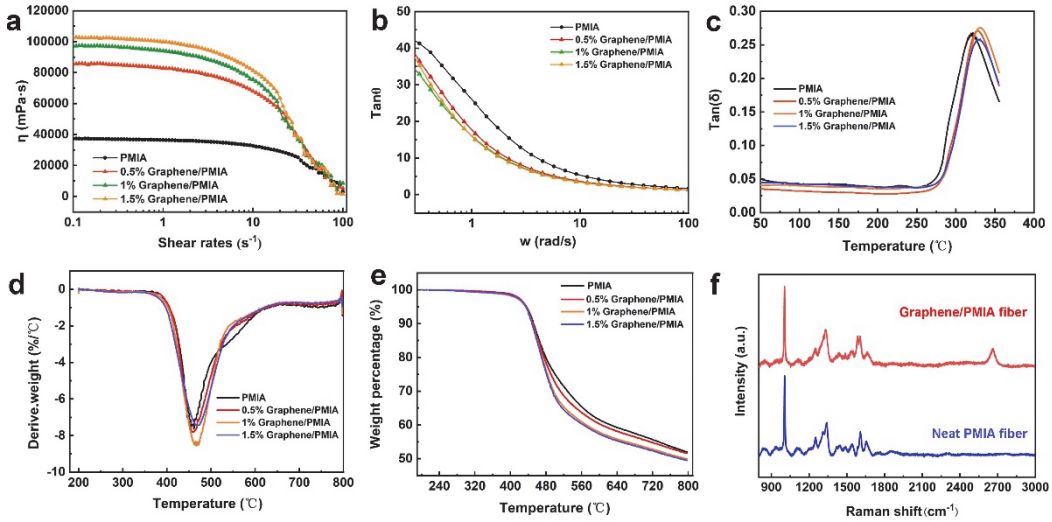

Fig. 3 (a) Steady-state rheological behaviors and (b) loss factor of neat PMIA and graphene/PMIA solution at 40 °C; (c) DMA curves of PMIA and graphene/PMIA blend fibers; (d) DTG curves, (e) TG curves and (f) Raman spectra of PMIA and graphene/PMIA fibers.

Therefore, when studying the impact of graphene on the rheological properties of PMIA polymers, it's essential to concentrate primarily on the interaction between graphene and PMIA polymer molecules. We achieved this through physical blending of graphene with a PMIA polymeric solution, resulting in an interface governed mainly by π–π interactions and hydrogen bonds between graphene and the benzene ring structure of the PMIA molecular chain. Some work has also revealed that graphene size significantly affects the rheology of polymer matrices [29]. The sub-micron scale graphene fabricated by MPCVD method is effortlessly entangled in the PMIA polymer chains, enabling excellent dispersion of graphene sheets in the polymer matrix.

The increased viscosity of the spinning dope might help align the graphene nanosheets along the fiber direction during the stretching process due to larger shear stress. Therefore, we can infer that the well-aligned graphene nanosheets guide the solidification of PMIA molecules during the coagulation process, helping minimize the large pores and voids. In Fig. 3a, due to the effective dispersion of graphene, the constructed graphene/PMIA polymer interface and interaction will hinder the movement of PMIA polymer molecules to a certain extent and increase the polymer viscosity. The loss factor represents the ratio of the viscosity to the elasticity of the polymer solution, and the smaller the loss factor, the greater the elasticity ratio of the polymer solution. The greater the elasticity ratio of the spinning solution, the greater the stretching ratio it can achieve. In Fig. 3b, compared with the pure PMIA polymer solution, the loss factor of all graphene/PMIA blend polymer solutions is reduced, that is, the elasticity of the blend solution is increased compared with the pure PMIA solution. The addition of graphene makes the molecular chains in the blend solution more closely combined, thereby increasing the elasticity of the blend solution. In addition, due to the weak interaction between graphene and PMIA molecular chains, and the size of graphene nanosheets being small enough to hinder the formation of microscopic entanglement on PMIA molecular chains, the blending polymer solution still has the shear thinning characteristic of the pseudoplastic fluid, which can ensure the smooth molding of the blended polymer. The uniform dispersion of graphene in the spinning solution is the premise for the excellent performance of the spun fibers.

Fig. 3c shows the dynamic thermodynamic curves of pure PMIA fibers and graphene/PMIA fibers, and the corresponding results are shown in Table 1. The glass transition temperature (T_g) of the blended fibers is higher than that of pure PMIA fibers, and the highest T_g of 1% graphene/PMIA is about 330 °C. The existence of graphene can effectively improve the crystallinity and orientation of the blended fibers during the thermoforming process. During the transition of the blended fibers from the highly elastic state to the glassy state, the graphene sheets can also limit the mutual sliding of the PMIA molecular chains to a certain extent and increase the intermolecular interactions. Therefore, the blended fibers will have a higher T_g. PMIA fibers are the most used heat-resistant fibers, we hope to modify PMIA fiber while maintaining its excellent heat resistance. We tested the thermal stability of graphene/PMIA fibers. The specific results are summarized in Table 1. It can be seen from the DTG

Table 1 T_g, T_c, and LOI of PMIA fiber and graphene/PMIA fiber.

Sample	PMIA	0.5% graphene/PMIA	1% graphene/PMIA	1.5% graphene/PMIA
T_g/°C	319	326	333	329
T_c/°C	461	464	468	471
LOI/%	28.2	28.2	28.4	28.5

(derivative thermogravimetric analysis) curve in Fig. 3d that the PMIA fibers begin to decompose at around 425 °C, and the thermal decomposition temperature of graphene/PMIA fibers is very close to that of the PMIA fibers. Therefore, the thermal resistance of the blend fibers is not affected by the addition of graphene. This is because the graphene addition will not change the molecular chain structure and molecular weight of PMIA, nor will it affect the decomposition process of the PMIA molecular chain inside the blended fibers. The increase in T_e may be due to better interfacial interaction between the PMIA matrix and graphene, which restricts the mobility of cellulose chains and thus delays the rate of thermal degradation. Furthermore, temperature at maximum decomposition rate (T_e) of graphene/PMIA fiber gradually increased due to the homogeneous dispersion, the barrier effect of nanolayered structure, and the high thermal stability of graphene. In addition, it can be seen from the TG (thermogravimetry) curve in Fig. 3e and Table 1 that compared with pure PMIA, the T_e of graphene/PMIA fibers increased to a certain extent, and T_e gradually increased with the increasing graphene content in graphene/PMIA fibers. This may be because the addition of graphene limits the degradation of PMIA molecular chains. With the increase of graphene addition, more PMIA molecular chains are restricted, which leads to the gradual increase of its T_e. The Raman spectra of PMIA fiber and graphene/PMIA fiber are shown in Fig. 3f. In addition to the Raman characteristic peaks of PMIA fibers (such as the peak at 1001 cm^{-1} related to the breathing vibration of the triangular ring of the m-benzene ring, which is also the highest intensity mode of neat PMIA), we can observe the existence of graphene's G' peak in the Raman spectrum of graphene/PMIA fiber, proving the existence of graphene in PMIA [30–32]. As shown in Table 1that the loss on ignition (LOI) of PMIA fibers is approximately 28.2%. The addition of graphene leads to an increase in the LOI values for the blended fibers. This could potentially be attributed to the densification of the fiber structure by graphene which may reduce its exposure surface to oxygen, thus slowing down degradation. Graphene may also enhance thermal conductivity which could mitigate the accumulation of heat at specific regions. In regards to ultraviolet radiation, the breaking of amide bonds results in reduced mechanical properties of PMIA fiber. Our study also aimed to assess the impact of graphene on PMIA fiber's UV resistance. According to data from Table S1 we found that incorporating 1 wt% graphene into PMIA fibers resulted in enhanced tensile strength retention and elongation at break, compared to pure PMIA fibers, following nine days of UV exposure. This improvement is likely attributable to the densification effect of graphene on the PMIA fiber structure as well as its role as a barrier against UV radiation penetration. The fabric made of PMIA fibers must have good moisture absorption and sweat wicking function. The contact angle of the fibers shown in Fig. S9 shows that the hydrophilicity of composite fibers is better than that of pure PMIA, indicating that composite fibers have good wearability.

Fig. S10 shows the good color uniformity and brightness of the as-spun and heat-drawn graphene/PMIA filament bundles, and the optical and polarizing microscope photos (Fig. S11) of the graphene/PMIA monofilament also exhibit its smooth and tubular shape with uniform fineness. The mechanical properties of PMIA fibers can be upgraded by the addition of graphene, as shown in Fig. 4a, typical tensile experiments of PMIA and graphene/PMIA fiber filament with 1 wt% graphene content show that the addition of graphene can extremely improve the breaking strength and elongation at break of PMIA as-spun fibers and heat-drawn fibers. The effects of graphene contents on the mechanical properties of PMIA as-spun fibers and heat-drawn fibers are shown in Fig. 4b and c, respectively. After heat treatment, under the 1 wt% graphene addition, the mean

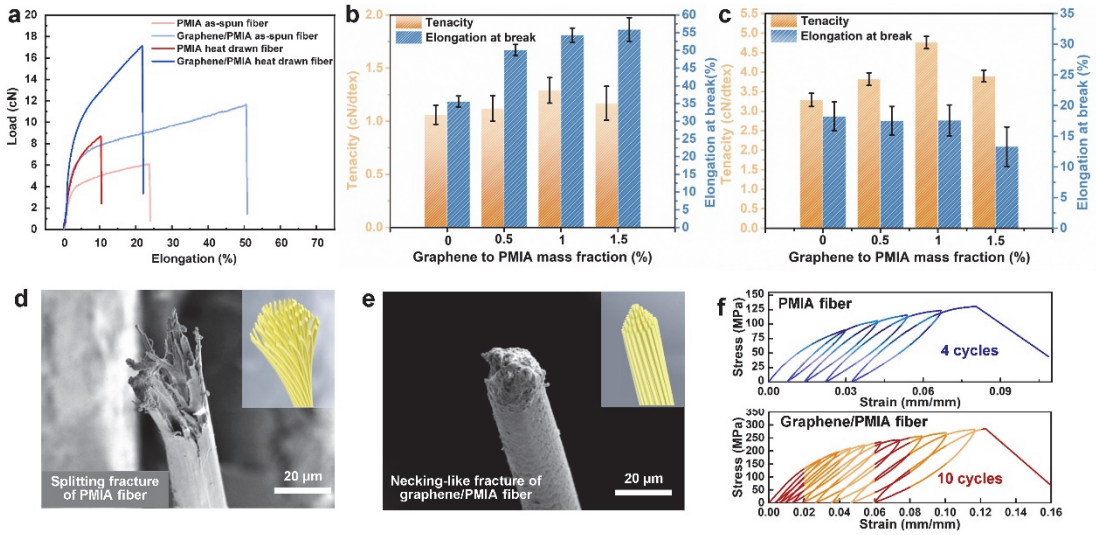

Fig. 4 (a) Typical stress−strain curves of PMIA fiber and graphene/PMIA fiber; Mean maximum tensile strength and elongation at break of as-spun (b) and heat-drawn (c) graphene/PMIA fibers with different graphene contents; Comparison of tensile fracture morphologies of PMIA fiber (d) and graphene/PMIA fiber (e); (f) Stress−strain curves of PMIA fiber and graphene/PMIA fiber under quasi-static cyclic loading conditions.

maximum breaking strength of PMIA fibers can reach 4.75 $cN \cdot dtex^{-1}$, and the mean elongation at break remains at the level of 17.5%. Compared with neat PMIA fibers, the breaking strength was increased by 46%. The stretching process parameters of graphene /PMIA fibers are shown in Table S2. With the increase of graphene content, PMIA fiber can withstand a greater tensile ratio. As shown in Fig. S12, an increased tensile ratio also makes graphene /PMIA fiber possess greater tensile strength. Fig. 4b,c show that the mechanical properties improvements of graphene/PMIA fibers after heat treatment are more obvious than those of as-spun fibers, indicating that the heat-drawn graphene/PMIA fibers have more crystalline regions and optimized internal orientation.

The graphene additions not only affect the ultimate mechanical properties of the PMIA fiber under a single stretch but also has a significant impact on its fatigue resistance under cyclic loading. We performed quasi-static cyclic micro-nano tensile experiments on neat PMIA fibers and graphene/PMIA fibers, respectively. The specific loading parameter settings are shown in Table S3. Fig. 4f presents the quasi-static cyclic loading fracture curves of neat PMIA fiber and graphene/PMIA fiber with 1.5 wt% graphene content. It can be seen that the ultimate strength and fracture strain of graphene/PMIA fibers under cyclic loading increase with the addition of graphene contents.

Similar to the tensile deformation curve of graphene/PMIA fiber under single loading, the stress-strain curve under cyclic loading can also be divided into three stages: elastic deformation, plastic deformation, and fracture damage. Notably, while improving the elastic modulus, breaking strength, and ultimate elongation of the fibers, the addition of graphene enables the residual strain of the graphene/PMIA fibers to be controlled under cyclic loading. When the graphene addition amount is 1 wt%, the residual strain of graphene/PMIA fibers after four cycles is only 1%. This is a 68% reduction in residual strain compared to neat PMIA fibers. For further understanding, we observed the fracture morphology of PMIA fibers and graphene/PMIA fibers after cyclic loading by SEM. From Fig. 4d, we can see that the fiber fracture is frizzy, and the fracture diameter is almost the same as that of the fibril. The plastic deformation and residual strain displayed during the entire fiber fracture process seem to be the cumulative performance of the uneven microstructure inside the fiber that is brittle fracture one by one. The resulting macroscopic phenomenon is the unique splitting fracture behavior of aramid fibers. The fiber fracture shown in Fig. 4e has obvious diameter shrinkage, showing obvious plastic fracture characteristics, and this plastic fracture characteristic varies with the amount of graphene addition. The π–π interactions and hydrogen bonds between graphene and PMIA molecular chains can effectively improve the density of PMIA fibers. As shown in the insets in Fig. 4d,e, the enhanced internal force can make PMIA molecules and their nanofiber structures more compact. Concentrating on bearing stress in the axial direction can effectively improve the comprehensive breaking strength on the one hand, and in addition, the change of such breaking behavior can also effectively improve the elongation at the break of the fibers.

2D-WAXD analysis was conducted to examine the crystal

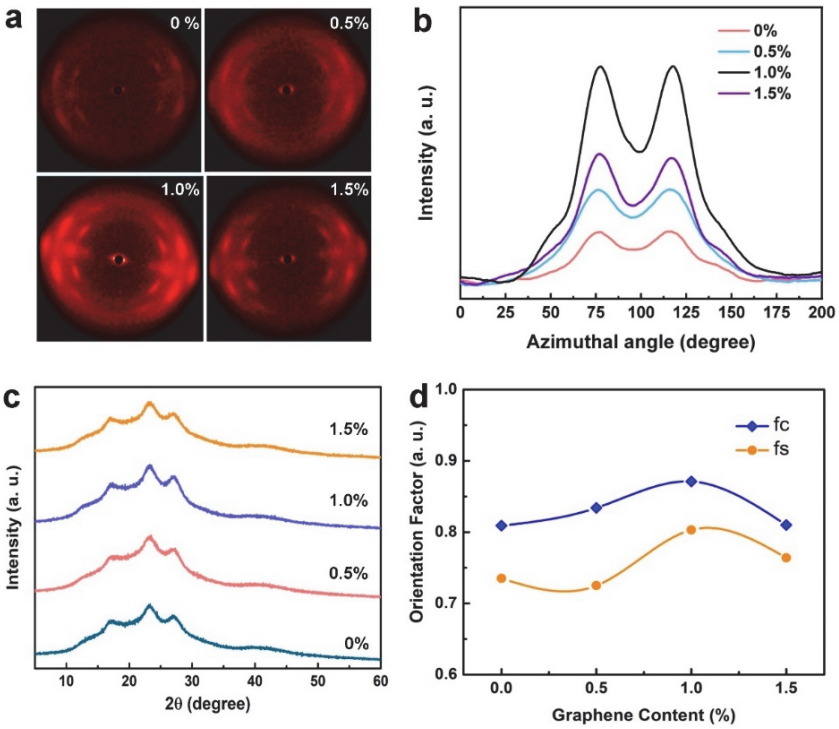

Fig. 5 (a) 2D-WAXD pattern of PMIA fibers with different graphene contents; (b) The azimuthal scan profiles of 2D-WAXD patterns in the panel; (c, d) XRD diagrams and orientation degrees of PMIA fibers with different graphene contents.

Table 2 Crystallinity of PMIA fibers and PMIA/graphene fibers.

Sample	PMIA	0.5% graphene/PMIA	1% graphene/PMIA	1.5% graphene/PMIA
Crystallinity/%	17.75	18.36	20.66	17.67

structure of graphene/PMIA fibers. As depicted in Fig. 5a, the two-dimensional diffraction patterns of PMIA fibers with varying graphene concentrations were obtained. The azimuthal intensity of the reflection at $2\theta = 23.3°$ is shown in Fig. 5b. The peak width at half height gradually reduces with the increase of graphene contents, indicating the improvement of orientation along the fiber direction. The degree of molecular orientation of the PMIA fibers is calculated based on the Hermans equation and is shown in Table S4. The orientation degree of neat PMIA fibers and graphene/PMIA fibers was computed and plotted in Fig. 5d. Results indicate that the orientation degree of graphene/PMIA fibers initially increases and subsequently decreases as the graphene content increases. When the graphene concentration reached 1.0 wt%, the orientation degree attained its maximum value of 0.871. Graphene (1.0 wt%) promoted optimum orientation and organized crystallization of PMIA molecular chains, leading to the highest degree of orientation. A minor quantity of graphene acted as a lubricant to encourage molecular chain regulation, but excessive amounts hindered the movement of molecular chains, impeding crystallization. In Fig. 5c, three prominent peaks located around $2\theta = 17.8°$, 23.3°, and 27.3° correspond to PMIA fibers. The crystallinity data of the 23.3° peak are provided in Table 2. Crystallinity improved steadily with rising graphene content, indicating that graphene might function as a nucleating agent during the PMIA crystallization process. Diffusion slowed down with escalating graphene content, facilitating the creation of crystalline domains within aggregate structures. Additionally, significant quantities of residual solvent remaining in the fibers served as lubricants, enhancing the mobility of polymer chains and fostering crystallization. Nonetheless, as graphene concentration increased further, the regular crystalline structure and efficient orientation of graphene/PMIA fibers tended to degrade, resulting in continually augmented crystallization and reduced orientation degrees.

4 Conclusions

This research explored the incorporation of graphene produced *via* microwave CVD into PMIA fibers. The evenly dispersed graphene sheets enhanced the internal structural integrity of graphene/PMIA fibers and elevated their mechanical properties. Our experimental outcomes demonstrated that adding 1 wt% graphene resulted in an improvement of up to 46% in the fiber's tensile strength. By reducing the number of internal imperfections and voids within the PMIA fibers, the integration of graphene led to a more condensed structural arrangement. Furthermore, the inclusion of graphene not solely impacted the material's resistance to static stress loads but also augmented its endurance against repeated loading cycles. Through SEM observations of fractured fibers containing varied amounts of graphene, it became evident that graphene modifies PMIA fibers exhibited clear signs of plastic deformation. Moreover, the XRD examination revealed that the addition of graphene improved both the crystallinity and orientation of the fibers. These discoveries provide valuable insight into developing advanced fiber materials with superior mechanical performance.

Author Contributions: Conceptualization, Z.G. and J.Z.; Methodology, Q.S., Z.G. and J.Y.; Investigation, Z.G., Q.S., and Z.X.; Characterization, Q.S., Z.L., T.L. and J.L.; Data analysis, Z.G., W.Z. and L.L.; Writing – Original Draft Preparation, Z.G., Q.S., S.W., and Z.X.; Writing – Review & Editing, Z.G., Q.S., and Z.X.; Supervision, J.Y. and J.Z.; Funding Acquisition, J.Z. and Z.G.

Supporting Information: available free of charge *via* the internet at https://www.whxb.pku.edu.cn.

References

(1) Tan, J.; Luo, Y.; Zhang, M.; Yang, B.; Li, F.; Ruan, S. *ACS Appl. Mater. Interfaces* **2021,** *13* (14), 16895. doi: 10.1021/acsami.1c02075

(2) Pegoretti, A.; Traina, M. *Handbook of Properties of Textile and Technical Fibres,* 2nd ed.; Elsevier: Cambrige, United States, 2018; pp. 621–697.

(3) Tang, C.; Li, X.; Li, Z.; Tian, W.; Zhou, Q. *Polymers* **2018,** *10* (12), 1348. doi: 10.3390/polym10121348

(4) Nazaré, S. *Advances in Fire Retardant Materials,* 1st ed.; Elsevier: Cambrige, United States, 2008; pp. 492–526

(5) Patel, A.; Wilcox, K.; Li, Z.; George, I.; Juneja, R.; Lollar, C.; Lazar, S.; Grunlan, J.; Tenhaeff, W.; Lutkenhaus, J. *ACS Appl. Mater. Interfaces* **2020,** *12* (23), 25756. doi: 10.1021/acsami.0c03671

(6) Horrocks, A.; Nazaré. S.; Masood, R.; Kandola, B.; Price, D. *Polym. Adv. Technol.* **2011,** *22*, 29. doi: 10.1002/pat.1707

(7) Li, X.; Tang, C.; Wang, J.; Tian, W.; Hu, D. *J. Mater. Sci.* **2019,** *54*, 8556. doi: 10.1007/s10853-019-03476-x

(8) Kang, W.; Deng, N.; Ma, X.; Ju, J.; Li, L.; Liu, X.; Cheng, B. *Electrochim. Acta* **2016,** *216*, 276. doi: 10.1016/j.electacta.2016.09.035

(9) Lu, Z.; Si, L.; Dang, W.; Zhao, Y. *Compos. Part. A-Appl. Sci. Manuf.* **2018,** *115*, 321. doi: 10.1016/j.compositesa.2018.10.009

(10) Ramani, R.; Kotresh, T.; Shekar, R. I.; Sanal, F.; Singh, U.; Renjith, R.; Amarendra, G. *Polymer* **2018,** *135*, 39. doi: 10.1016/j.polymer.2017.11.064

(11) Yang, C.; Wu, H.; Dai, Y.; Tang, S.; Luo, L.; Liu, X. *Polymer* **2019,** *180*, 121687. doi: 10.1016/j.polymer.2019.121687

(12) Chung, J.; Kwak, S. *Eur. Polym. J.* **2018,** *107*, 46. doi: 10.1016/j.eurpolymj.2018.07.051

(13) Fei, B. *Engineering of High-Performance Textiles,* 1st ed.; Elsevier: Cambrige, United States, 2018; pp. 27–58.

(14) Lee, C.; Wei, X.; Kysar, J. W.; Hone, J. *Science* **2008,** *321*, 385. doi: 10.1126/science.1157996

(15) Suk, J.; Piner, R.; An, J.; Ruoff, R. *ACS Nano* **2010,** *4*, 6557. doi: 10.1021/nn101781v

(16) Ramanathan, T.; Abdala, A.; Stankovich, S.; Dikin, D.; Herrera-Alonso, M.; Piner, R.; Adamson, D.; Schniepp, H.; Chen, X.; Ruoff, R.; *et al*. *Nat. Nanotechnol.* **2008,** *3*, 327. doi: 10.1038/nnano.2008.96

(17) Fan, J.; Shi, Z.; Zhang, L.; Wang, J.; Yin, J. *Nanoscale* **2012,** *4*, 7046. doi: 10.1039/C2NR31907A

(18) Yang, Z.; Jin, L.; Lu, G.; Xiao, Q.; Zhang, Y.; Jing, L.; Zhang, X.; Yan, Y.; Sun, K. *Adv. Funct. Mater*. **2014,** *24*, 3917. doi: 10.1002/adfm.201304091

(19) Sun, K.; Dong, H.; Kou, Y.; Yang, H.; Liu, H.; Li, Y.; Shi, Q. *Chem. Eng. J.* **2021,** *419*, 129637. doi: 10.1016/j.cej.2021.129637

(20) Chen, S.; Wu, Q.; Mishra, C.; Kang, J.; Zhang, H.; Cho, K.; Cai, W.; Balandin, A.; Ruoff, R. *Nat. Mater.* **2012,** *11*, 203. doi: 10.1038/nmat3207

(21) Stöberl, U.; Wurstbauer, U.; Wegscheider, W.; Weiss, D.; Eroms, J. *Appl. Phys. Lett*. **2008,** *93*, 051906. doi: 10.1063/1.2968310

(22) Zhang, B.; Lian, T.; Shao, X.; Tian, M. *Ind. Eng. Chem. Res.* **2021,** *60*, 2472. doi: 10.1021/acs.iecr.0c05794

(23) Sun, Y.; Chen, Z.; Gong, H.; Li, X.; Gao, Z.; Xu, S.; Han, X.; Han, B.; Meng, X.; Zhang, J. *Adv. Mater.* **2020,** *32*, 2002024. doi: 10.1002/adma.202002024

(24) Zeng, L.; Liu, X.; Chen, X.; Soutis, C. *Compos. Part. B-Eng*. **2021,** *220*, 108983. doi: 10.1016/j.compositesb.2021.108983

(25) Luo, T.; Lloyd, J. *Adv. Funct. Mater*. **2012,** *22*, 2495. doi: 10.1002/adfm.201103048

(26) Song, Q.; Wu, W.; Wang, Y.; Yu, J.; Hu, Z.; Wang, Y. *Adv. Fiber. Mater*. **2022,** *4*, 436. doi: 10.1007/s42765-021-00110-x

(27) Song, Q.; Feng, Y.; Wu, W.; Yu, J.; Hu, Z.; Wang, Y.; Zhu, J. *J. Text. Inst*. **2021,** *112*, 2004. doi: 10.1080/00405000.2020.1862491

(28) Sun, Y.; Yang, L.; Xia, K.; Liu, H.; Han, D.; Zhang, Y.; Zhang, J. *Adv. Mater.* **2018,** *30*, 1803189. doi: 10.1002/adma.201803189

(29) Moghaddam, M.; Goharshadi, E.; Entezari, M.; Nancarrow, P. *Chem. Eng. J.* **2013,** *231*, 365. doi: 10.1016/j.cej.2013.07.006

(30) Chazot, C.; Damirchi, B.; Lee, B.; Van Duin, A.; Hart, A. *Nano Lett.* **2022,** *22*, 998. doi: 10.1021/acs.nanolett.1c03866

(31) Edwards, H.; Hakiki, S. *Brit. Polym. J.* **1989,** *21*, 505. doi: 10.1002/pi.4980210611

(32) Malard, L.; Pimenta, M.; Dresselhaus, G.; Dresselhaus, M. *Phys. Rep.* **2009,** *473*, 51. doi: 10.1016/j.physrep.2009.02.003